SUPPLEMENTAL MATERIAL

Senescent phenotype induced by p90RSK-NRF2 signaling sensitizes monocytes and macrophages to oxidative stress in HIV$^+$ individuals: implications for atherogenesis

Meera V. Singh, PhD[2,12], Sivareddy Kotla, PhD[1,12], Nhat-Tu Le, PhD[1,9,12], Kyung Ae Ko, DVM[1,12], Kyung-Sun Heo, PhD[1,10], Yin Wang, PhD[1], Yuka Fujii, MD, PhD[1,11], Hang Thi Vu, PhD[1], Elena McBeath, PhD[1], Tamlyn N. Thomas, BS[1], Young Jin Gi, MS[1], Yunting Tao, MS[1,9], Jan L. Medina, MS[1], Jack Taunton, PhD[4], Nancy Carson, RDMS, RVT[5], Vikram Dogra, MBBS[5], Marvin M. Doyley, PhD[6], Alicia Tyrell, BS[7], Wang Lu, MS[7], Xing Qiu, PhD[7], Nicole E. Stirpe, BS[2], Kathleen J. Gates, BS[2], Christine Hurley, RN[8], Keigi Fujiwara, PhD[1], Sanjay B. Maggirwar, PhD[2,13], Giovanni Schifitto, MD, MS[3,13], and Jun-ichi Abe, MD, PhD[1,13]

[1]Department of Cardiology, The University of Texas MD Anderson Cancer Center, Houston, Texas, USA; [2]Department of Microbiology and Immunology, University of Rochester, Rochester, New York, USA; [3]Department of Neurology, University of Rochester, Rochester, New York, USA; [4]Department of Cellular and Molecular Pharmacology, University of California-San Francisco, San Francisco, California, USA; [5]Department of Imaging Sciences, University of Rochester, Rochester, New York, USA; [6]Department of Electrical and Computer Engineering, University of Rochester, Rochester, New York, USA; [7]Department of Biostatistics and Computational Biology, University of Rochester, Rochester, New York, USA; [8]Department of Medicine, Infectious Disease, University of Rochester, Rochester, New York, USA.

Current address:
[9]Department of Cardiovascular Sciences, Houston Methodist Research Institute, Houston, Texas, USA; [10]Institute of Drug Research & Development, Chungnam National University, Daejeon, Republic of Korea; [11]Department of Radiology-research, Houston Methodist Research Institute, Houston, Texas, USA

[12]These authors contributed equally to this work.

[13]These authors were equivalent co-senior authors.

Correspondence should be addressed to J.A. (jabe@mdanderson.org), S.B.M. (Sanjay_Maggirwar@URMC.Rochester.edu), or G.S. (Giovanni_Schifitto@URMC.Rochester.edu).

Running title: cART-induced p90RSK activation and atherosclerosis

Methods

The data, analytic methods, and study materials that support the findings of this study are available from the corresponding authors upon reasonable request.

Population studies

The study was approved by the Institutional Review Board of the University of Rochester.

The inclusion criteria for HIV-infected participants were as follows: 1) Seropositive for HIV-1 on the basis of documented HIV infection, 2) on stable cART for at least 12 months prior to screening, 3) viral load ≤200 copies/mL at screening, 4) capable of giving informed consent, 5) age ≥45 years, and 6) the following laboratory values within 30 days prior to entry: hemoglobin >9.0 g/dL, AST (SGOT), ALT (SGPT), and alkaline phosphatase <2 x ULN.

The exclusion criteria for HIV^+ participants were as follows: 1) symptomatic CVD (angina, myocardial infarction, stroke, or other peripheral atherosclerotic disease); 2) uncontrolled diabetes mellitus, uncontrolled hypertension, or familial hypercholesterolemia; 3) current use of immunosuppressants, 4) current use of oral hormone therapy; 5) chronic inflammatory conditions, such as severe arthritis, lupus, or inflammatory bowel disease; 6) alcohol abuse (men: ≥15 drinks/week, women: ≥12 drinks/week, binge drinking: ≥5 drinks/day for men and ≥4 drinks/day for women) or drug abuse (except marijuana) within the past year (alcohol use was reported at patient screening, and a urine toxicology screen was collected at each visit; 7) uncontrolled hypothyroidism; 8) pregnancy; and 9) any medical condition that, in the opinion of the investigators, could compromise successful study participation.

Pregnancy risk was evaluated as follows: women who had experienced menarche and who had not undergone successful surgical sterilization, hysterectomy, bilateral tubal ligation, or bilateral oophorectomy; and were not postmenopausal (defined as amenorrhea >12 consecutive months) or on hormone replacement therapy with documented serum follicle stimulating hormone level >35 mIU/mL were considered to be childbearing potential and would undergo serial pregnancy tests during the study. A negative serum or urine pregnancy test with a sensitivity of at least 25 to 50 mIU/mL was required prior to screening. Age-matched HIV^- controls were enrolled using the same inclusion and exclusion criteria. Participants underwent a clinical and laboratory evaluation (lipid profile, CBC, chemistry, and hs-CRP) and Reynolds risk score assessment[1].

Missing values

No imputation was performed for baseline missing data.

Power analysis

We conducted two additional power analyses based on the empty and H_20_2-stimulated p90RSK data collected in this study. As shown in Fig. 1d, the mean H_20_2-stimulated p90RSK activation level was 9.500 for HIV^- participants (n=86) and 2.805 for HIV^+ participants (n=92), which represents a mean group difference of 6.694. In addition, the pooled standard deviation of the H_20_2-stimulated p90RSK activation level was 10.371. On the basis of these results, a power analysis showed that with ≥52 in each group, we would have more than 90% statistical power to reject the null hypothesis at a 0.05 significance level in a similarly conducted study. In comparison, we observed that the mean difference in the empty p90RSK activation levels between the HIV^+ subjects and controls was 0.841; the

corresponding pooled standard deviation was 9.286. On the basis of these findings, a power analysis showed that we would not have 90% or more statistical power unless there were ≥2,558 subjects in each group, which is certainly impractical; this finding corroborates our earlier conclusion that the observed group difference of empty p90RSK activation level was not statistically significant (p=0.537).

Of note, this cross-sectional study is part of an ongoing longitudinal study. An initial power analysis was performed on the basis of this longitudinal analysis. We reported this cross-sectional analysis because of interesting findings regarding H_20_2-induced p90rsk activity. On the basis of the STROBE guideline requirements, we have provided our post hoc analysis; however, we emphasize that this practice may have some limitations, as it has been reported previously[2].

Observer blinding
This was part of a longitudinal observational study. The laboratory that assessed p90RSK levels and the sonographer were blinded to each other's findings and to the submitted data (p90RSK and the presence of carotid plaques) independently and separately for entry into the database.

Carotid plaque evaluation in humans
The ultrasound scanner used was the Sonix RP L14-5 Mhz linear array with harmonics setting 7 Mhz (http://www.ultrasonix.com/wikisonix/index.php/Sonix_RP). This is a diagnostic ultrasound system packaged with an Ultrasound Research Interface. An experienced sonographer, supervised by an ultrasound specialist (Dr. Dogra), performed the ultrasound evaluations. All ultrasound scans were read by the same sonographer. Both left and right extra-cranial carotids were assessed for the presence of plaques. The presence of plaques was defined as the presence of focal wall thickening by visual inspection. Quantification in a random subset showed that the focal thickness was at least 50% greater than that of the surrounding vessel wall and the intima-media thickness was greater than 1.5 mm, consistent with the American Society of Echocardiography recommendation[3].

Antibodies and reagents
The following antibodies were acquired: anti-p16 (orb228122; Biorbyt, San Francisco, CA), anti-phospho-ERK5 S496 (A02812; Boster Bio, Pleasanton, CA), anti-NRF2 (GTX103322; Genetex, Irvine, CA), anti-thioredoxin (Trx1) (14999-1 AP20; Proteintech, Rosemont, IL), anti-p90RSK (MAB 2056; R&D Systems, Minneapolis, MN), and anti-α-tubulin (T5168; Sigma-Aldrich, St. Louis, MO). In addition, antibodies against phospho-ERK5 TEY (3371), ERK5 (3372), phospho-p90RSK (9341), and p21 (2947), and anti-cleaved caspase-3 (9661) were purchased from Cell Signaling Technology (Beverly, MA), anti-CD36 (9156), anti-Gas6 (SC9035), anti-heme oxygenase 1 (HO1) (SC-10789), anti-TNFα (SC-33165), anti-VE-cadherin (SC-48), and anti-VCAM-1 (H-276, SC-8304) were from Santa Cruz (Santa Cruz, CA), and anti-VE-cadherin (BD555289) from BD Biosciences. Protease inhibitor cocktail (p8340), PMSF (36978), and NEM (E3876) were purchased from Sigma-Aldrich (St. Louis, MO). The lipid profile kit (ab65390) and MitoTEMPO (ab144644) were from Abcam (Cambridge, MA); the iQSYBR Green Supermix (1708882) and iScript cDNA synthesis kits (1708890) were from Bio Rad (Hercules, CA); and elvitegravir (GS-9137) and raltegravir (MK-0518) were from Selleckchem (Houston, TX).

We also used an ARE reporter kit (60514; BPS Biosciences, San Diego, CA), a telomere (TL) PNA kit/FITC flow cytometry kit (K5327; Agilent Technology, Santa Clara, CA), a chemiluminescence detection reagent kit (NEL105001EA; PerkinElmer, Waltham, MA), an ApopTag peroxidase *in situ*

apoptosis detection kit (S7100; Millipore, Burlington, MA), TaqMan reverse transcription reagents (N808-0234; Applied Biosystems, Foster City, CA), an efferocytosis kit (4649; Essen Biosciences, Ann Arbor, MI), an NRF2 activator (492042; Calbiochem, Kenilworth, NJ), and Lipofectamine 2000 transfection reagent (11668027; ThermoFisher Scientific, Waltham, MA). Tenofovir (TDF), emtricitabine (FTC), atazanavir sulfate (ATV), ritonavir (RTV), maraviroc (MVC), efavirenz (EFV), and rilpivirine (RPV) were obtained from the NIH AIDS Reagent Program (Germantown, MD 20874, USA). Except FTC and MVC (dissolved in PBS) all drugs were dissolved in DMSO, and final concentration of DMSO in cell culture was 0.1%, which we used as a vehicle control. Each drug concentration used in this study was within the therapeutic range of plasma concentration in humans, as reported previously[4-10], or based on the maximum concentration (Cmax) and the area under the curve (AUC) data, which are also available from the information on each drug manufacturer's site.

Human whole blood processing and flow cytometry

All blood samples were processed within 3 h of blood draw. We fixed 100 μL of blood with an equal volume of 4% paraformaldehyde (PFA, EM Sciences, PA, USA) for 15 min in the dark at room temperature (RT). Alternatively, 100 μL of blood was treated with 200 μM of H_2O_2 for 4 min at RT and then fixed with 4% PFA. The blood was washed twice with 1 mL of IC permeabilization buffer (Invitrogen, CA, USA) followed by staining with titrated volumes of antibodies against CD14-PE (8 μL), RSK-1-AF647 (5 μL), and phospho-p90RSK-AF488 (2 μL) for 30 min at 4°C in dark. The cells were washed with IC permeabilization buffer and then washed with PBS. Unstained cells, cells stained with CD14 only, and cells stained with $CD14^+$ RSK were used as fluorescence minus one controls. Each sample was acquired using an Accuri C6 flow cytometer (BD Biosciences, CA, USA) at slow speed. We acquired 50,000 events per samples in the "Leukocyte" gate, as per forward and side scatter characteristics. FlowJo software (version 10.4.1, FlowJo LLC, USA) was used to analyze the data. VersaComp antibody capture beads (#B22804, Beckman Coulter, CA, USA) were used to calculate the compensation matrix.

Repeatability of p90RSK activity measurement by using flow cytometry

On the basis of the STROBE guideline requirements, we determined the repeatability of the p90RSK activity (i.e. phosphorylation: Ph) measurement in human whole blood samples. Whole blood from one HIV uninfected healthy individual was treated with five different doses ranging from 100-500 μM H_2O_2 for 4 min at room temperature. Alternatively, blood was treated with 200 μM H_2O_2 at different time points from 0 - 16 min. All treatments were performed in triplicate and used to measure p90RSK activation by flow cytometry. As shown in Supplemental Fig.10, p90RSK activity measurement was very repeatable.

Generation of plasmids and adenoviruses

Plasmids containing rat wild-type (WT) p90RSK1 (WT-*p90rsk*) (Genebank NM031107) and dominant-negative (kinase dead) *p90rsk1* with K94A/K447A mutations (DN-*p90rsk1*) were generated as previously described by us[11]. Gal4-ERK5 was created by inserting mouse ERK5 isolated from the pcDNA3.1-ERK5 vector into BamH1 and Not1 sites of the pBIND vector. An adenovirus vector containing constitutively active (CA)-MEK5α was subcloned into the pENTR vector (Invitrogen), and a recombinase reaction was performed to obtain a pDEST-based vector, following the manufacturer's instructions (K4930-00, ViraPower Adenoviral Expression System, Promega). All constructs were

verified by DNA sequencing using vector-specific primers. Where indicated, adenovirus containing β-galactosidase (Ad-LacZ) was used as a control.

Human and mouse monocyte and macrophage culture
Normal human peripheral blood CD14+ monocytes (ATCC PCS-800-010) were purchased from the American Type Culture Collection (ATCC, Manassas, VA); suspended in Iscove's modified Dulbecco's medium (IMDM) (#13390, Sigma-Aldrich) containing 10% fetal bovine serum (FBS) (v/v; Hyclone), 1% HEPES (15630080, ThermoFisher), and 1% penicillin-streptomycin (15140122, ThermoFisher); and immediately used in the experiments. Bone marrow-derived macrophages (BMDMs) were cultured as follows: monocytes isolated from the femurs and tibias of mice from C57BL/6 or various transgenic mice on C57BL/6 background were differentiated to macrophages by incubating the cells at a density of $1x10^6$ cells/mL in IMDM containing 10% FBS, 10% (v/v) of the spent medium of L929 cell cultures as the source of macrophage colony stimulating factor[12], 1% HEPES, and 1% penicillin-streptomycin for 5-8 days at 37˚C and 5% CO_2 in air. Peritoneal neutrophils and macrophages were obtained after an i.p. injection of 2 mL of autoclaved 3% (w/v) thioglycolate in H_2O (Sigma-Aldrich). After 3 days, peritoneal cells were harvested by injecting 10 mL of DMEM containing 10% FBS into the peritoneal cavity; the abdomen was gently massaged to dislodge cells, and the cell suspension was collected. The mouse monocyte and macrophage cell line RAW264.7, was obtained from ATCC (TIB-71) and propagated in DMEM containing 10% FBS at 37˚C and 5% CO_2 in air.

Transfection and transduction
Cells were transfected with the appropriate plasmid DNAs using Lipofectamine 2000 transfection reagent, according to the manufacturer's instructions. After transfection, cells were allowed to recover in the complete medium for 24 h. For adenovirus transduction, we used 10 multiplicity of infection (MOI). Prior to use, cells were cultured overnight in a low-serum (1% FBS) medium.

Western blotting analysis
Macrophages were washed twice with cold PBS, and whole cell lysates were prepared in RIPA buffer (50 mM Tris-HCl [pH 7.4], 150 mM NaCl, 1 mM EDTA, 1% Nonidet P40, 0.1% SDS, 1 mM dithiothreitol, 1:200-diluted protease inhibitor cocktail [P8340, Sigma-Aldrich], and 1 mM PMSF). Total lysates were resolved by SDS-PAGE and electrotransferred onto a Hybond enhanced chemiluminescence nitrocellulose membrane, which was incubated with antibodies against each of the proteins to be detected in the lysate. Bound antibodies were visualized using the enhanced chemiluminescence detection reagents (Amersham Pharmacia Biotech), according to the manufacturer's instructions, and quantified by densitometry using ImageJ software. Tubulin was used as the loading control and was always probed together with the specific protein of interest. The immunoblotted band intensities of the proteins of interest were standardized against the intensity of the anti-tubulin band. In most cases, anti-tubulin immunoblots are not shown to save space.

Real-time polymerase chain reaction
The cell lysates were loaded onto the QIAShredder column (QIAShredder kit; 79656, QIAGEN Sciences) and spun down to obtain the supernatant. Total RNA was then isolated using the RNeasy Plus Mini Kit (74136, QIAGEN Sciences), following the manufacturer's instructions. cDNA reverse transcription was performed in 50 μL of reaction mixture containing 1 μg of purified RNA, 5 μL of

10X buffer, 11 μL of $MgCl_2$, 10 μL of dNTPs, 2.5 μL of random hexamer, 1.25 μL of oligo dT, 1 μL of RNAse inhibitor, and 0.75 μL of TaqMan reverse transcription reagents (N808-0234, Roche Molecular Systems). For real-time polymerase chain reaction (RT-PCR), we purchased mouse primers, including Mertk (MP202617), gas6 (MP205762), and Mfg-e8 (MP208190), from Origene with qSTAR qPCR primers. In addition, specific primers were designed using Primer Express 3.0 software (Supplemental Table 5). Quantitative RT-PCR was performed using the MyiQTM2 two-color real-time PCR system (Bio-Rad) and SYBR Green (Bio-Rad) to measure gene expression. The cycling program was set as follows: thermal activation for 10 min at 95°C and 40 cycles of PCR (melting for 15 s at 95°C, followed by annealing/extension for 1 min at 60°C). Specific gene expression data were normalized to GAPDH gene expression.

ERK5 transcriptional activity

RAW264.7 and BMDMs were plated on 12-well plates at $5x10^4$ cells/well. To detect ERK5 transcription activity, we transfected cells with Gal4-ERK5 and the Gal4-responsive luciferase reporter pG5-*luc* in Opti-MEM containing Lipofectamine 2000, per the manufacturer's instructions. The pG5-luc vector contains five Gal4 binding sites upstream of a minimal TATA box, which in turn, is upstream of the firefly luciferase gene. pBIND-containing Gal4 was fused with p90RSK, and pACT containing VP16 was fused with either full-length ERK5. Since pBIND also contains the *Renilla* luciferase gene, expression and transfection efficiencies were normalized to Renilla luciferase activity. Opti-MEM was replaced by fresh complete culture medium 4 h after transfection. After 16 h of transfection, cells were stimulated by various cART regimens and then collected after 36 h of transfection to measure the luciferase activity with the dual luciferase kit (E1960, Promega) by a TD-20/20 luminometer (Turner Designs, CA). Transfections were performed in triplicate, and each experiment was repeated at least three times.

NRF2-ARE transcriptional activity

BMDMs were seeded on 12-well plates at $5x10^4$ cells/well and transfected using Opti-MEM, Lipofectamine 2000 with an ARE luciferase reporter, and constitutively expressing *Renilla* luciferase vectors (ARE reporter kit, BPSBioscience). After 16 h of transfection, cells were stimulated by various cART regimens and collected after 36 h of transfection to measure the luciferase activity with the dual luciferase kit (E1960, Promega) and a TD-20/20 luminometer (Turner Designs, CA), per the manufacturer's instructions. Transfections were performed in triplicate, and each experiment was repeated at least three times.

Efferocytosis assay

BMDMs were cultured in IMDM containing 10% FBS (v/v; Hyclone), 1% HEPES, and 1% penicillin-streptomycin. To induce apoptosis in these cells, we treated $1x10^6$ cells/mL in suspension with camptothecin (100 nM) for 6 h and labeled them with IncuCyte pHrodo Red cell-labeling reagents (250 ng/mL) for 1 h. For the efferocytosis assay, $1x10^4$ BMDMs (effector cells) were plated on a 96-well flat-bottom plate, and apoptotic cells were added to the surface of the adhered BMDMs. After incubating the cells for 1 h, efferocytotic activity was monitored using IncuCyte ZOOM live cell imaging (ESSEN Bioscience, Ann Arbor, MI). Engulfment of pHrodo-labeled cells induces pHrodo fluorescence by the acidic environment of the phagosome, and the fluorescence intensity of the image was determined using IncuCyte ZOOM.

TL length assay

TL length was measured using the TL PNA kit/FITC (DAKO, Glostrup, Denmark), per the manufacturer's instructions. In brief, BMDMs were suspended and washed by PBS, then incubated with the hybridization solution supplemented with or without the fluorescein-conjugated PNA TL probe, and heated to 82°C for 10 min. Hybridization was allowed to proceed in the dark at RT overnight. Cells were then washed twice, for 10 min each, using the washing solution supplied by the kit at 40°C. DNA staining solution provided in the kit was used to identify G0/1 cells for calculating the DNA index by dividing the mean of the G0/1 peak by the mean of the sample peak obtained from the DNA histogram[13]. Cells were resuspended in the DNA staining buffer and incubated for 1 h at RT. After being washed, the cells were analyzed by a BD Accuri C6 Flow Cytometer using the FL-1 channel to detect the FITC signal and the FL-3 channel for propidium iodide. The human 1301 cell line (T-cell leukemia, #01151619-1VL, Sigma-Aldrich) was used as a control because these cells have unusually long TLs. We cultured 1301 cells in RPMI 1640 containing 2 mM L-glutamine and 10% FBS, and the TL signal was measured as described above. Relative TL length was determined by calculating the ratio of the TL signal of each sample and that of 1301 cells after the correction for the DNA index of G0/1 cells for each cell type.

Measurements of intracellular reactive oxygen species levels

Intracellular ROS was measured by using the membrane-permeable oxidation-sensitive fluorescent dye, CM-H_2DCF-DA (5-(and-6)-chloromethyl-2',7'-dichlorodihydrofluorescein diacetate) from Invitrogen (#C6827, Invitrogen, Eugene, OR). Cells were seeded overnight in 96-well plates, washed with PBS, and incubated with CM-H_2DCF-DA (10 μM, 30 min). Fluorescence intensity was measured by a spectroflurometer using excitation at 495 nm and emission at 530 nm (Biotek, Winooski, VT).

Mitochondria specific reactive oxygen species measurements

Cells were washed with PBS and incubated with MitoSOX Red (5 μM) (#M36008, Invitrogen, Eugene, OR) at 37^0C for 10 min. Fluorescence intensity was measured with excitation at 510nm and emission at 580 nm using a plate reader (Biotek, Winooski, VT) as described in the manufacturer's instructions (Invitrogen). The mean intensity of MitoSOX fluorescence was normalized with that in control untreated cells, and the fold change in intensity was calculated.

Mice and left carotid artery partial ligation

Mice were maintained in the vivariums of the Texas A&M Institute of Bioscience and Technology and The University of Texas MD Anderson Cancer Center. All animal procedures were approved by the University Committee on Animal Resources of Texas A&M (2014-0231, 2017-0154) and the Institutional Animal Use and Care Committee of MD Anderson (00001652, 00001109). All animals were housed in a temperature-controlled room under a light (12 h)/dark (12 h) cycle and pathogen-free conditions.

Ldlr$^{-/-}$ and C57BL/6 mice were obtained from The Jackson Laboratory (Bar Harbor, ME). Eight- to twelve-week-old *Ldlr*$^{-/-}$ mice were fed an adjusted-calorie (high-fat) diet (HFD) consisting of 21% crude fat, 0.15% cholesterol, and 19.5% casein (cat. no. TD.88137; Envigo, NJ)[11] as indicated in each figure. For evaluating atherosclerotic plaque formation, male mice were used. The weight range of the mice was 20-25 g. Genotyping was performed on the basis of The Jackson Laboratory protocol, and we confirmed that the mice were homozygous. No previous procedures were performed before the experiments in this study. Rat p90RSK1 (Genebank NM031107) was mutated to K94A/K447A to

create a kinase-dead and dominant-negative form of p90RSK (DN-p90rsk), as we previously reported[14]. Myeloid cell-specific transgenic WT-*p90rsk*-MTg mice and DN-*p90rsk*-MTg mice were generated using mice expressing *Cre*-recombinase under the regulation of LysM promoter (C57BL/6 background). Genotyping of pups was performed by PCR of tail samples. For the atherosclerosis studies, WT-*p90rsk*-MTg mice were crossed with *Ldlr*$^{-/-}$ (C57BL/6J background) mice (WT-*p90rsk*-MTg/*Ldlr*$^{-/-}$). At 8 weeks of age, the mice were placed on a HFD for 12 or 16 weeks.

We obtained rAAV plasmids encoding gain-of-function forms of murine PCSK9 (pAAV/D377Y-mPCSK9) from Addgene (plasmid #58376)[15]. The expression of PCSK9 was driven by an efficient liver-specific promoter, HCEApoE/hAAT. Viral vectors in serotype 8 capsids rAAV8-D377Y-mPCSK9 were produced by the University of North Carolina Vector Core (Chapel Hill, NC). Viral vectors (1 x10^{11} titer/mouse) were delivered via a single tail vein injection into DN-*p90rsk*-MTg non-transgenic littermate control (NLC) or WT mice; these animals had been challenged with a HFD for 4 weeks, and partial left carotid artery (LCA) ligation was performed. In brief, three of the four caudal branches of the LCA (left external carotid, internal carotid, and superior thyroid artery) were ligated with 6–0 silk suture while the occipital artery was left intact[16]. To study the effect of cART on atherosclerosis, we treated *Ldlr*$^{-/-}$ mice with TDF (24.3 mg/kg/day), FTC (16.2 mg/kg/day), ATV (24.3 mg/kg/day), and RTV (8.1 mg/kg/day) or vehicle (DMSO, 1ml/kg/day) by intraperitoneal for 14 consecutive days 7 days after LCA ligation. The gross lesion (%) was detected by the ratio of the area of the plaque lesion and total LCA area, which were quantified using ImageJ software (http://imagej.nih.gov/ij/), as shown in Supplemental Fig. 10. We conducted a double-blind, randomized study, and the persons who evaluated the size of the plaques were blinded to the animals from which samples were made.

Monitoring of mice after surgery

Mice after the PCL surgery were monitored in a chamber on a heating pad and pre-warmed normal saline [37°C, 5 ml per 100 g body weight] was given subcutaneously. They were given postoperative analgesia as needed for additional pain relief. We checked on the mice every 10 minutes until they were awake and moving, and thereafter twice daily for the first 3 days (the date of surgery was day 1) and then once per week until the conclusion of the study, as described in our protocol approved by the Institutional Animal Use and Care Committee.

Histological examination and evaluation of atherosclerotic lesions after partial carotid ligation (PCL)

Four weeks after surgery, the LCA and right carotid artery (RCA) were harvested, fixed, embedded in paraffin, serially sectioned (5 μm), and stained with hematoxylin and eosin, as we described previously[17]. Plaque formation was evaluated by detecting the intima and media areas, which were quantified using ImageJ software (http://imagej.nih.gov/ij/), as we described previously[18]. The intima area was calculated by subtracting the lumen area from the area circumscribed by the internal elastic lamina, and the medial area was defined as the area between the internal and external elastic laminae. For evaluating the d-flow-induced plaque size after PCL, we calculated the ratio of LCA total area (intima + media) and RCA media area in the cross-sections obtained from 5-10 different locations along the carotid arteries.

Grading of necrotic core formation

To quantify necrotic core formation, we stained cross-sectioned carotid arteries with hematoxylin and eosin, and quantified the necrotic core formation by the percentage of non-cellular area/total lesion area by using ImageJ (http://imagej.nih.gov/ij/). We graded each necrotic core as no necrotic core = 0, ≤5% = 1 and >5 % = 2 and scored them at seven different levels within each carotid artery after partial carotid ligation as we described previously[18]. For each mouse, the sum of the total grades was calculated.

Immunofluorescence staining

Immunofluorescence staining was performed on paraffin slides, as described previously[19]. In brief, the tissue sections were de-paraffinized, and heat-induced epitope retrieval (HIER) was performed by boiling the sections in heat-induced epitope retrieval (HIER) buffer containing 10 mM sodium citrate and 0.05% Tween 20 (pH 6) for 20 min. The slides were first blocked by incubation with 10% normal goat serum for 1 h at RT and then incubated with primary antibodies (rabbit anti-Gas6 1:200 dilution, rabbit anti-TNFα 1:200 dilution, or rabbit anti-cleaved caspase-3 1:300 dilution or rabbit IgG) at 4°C overnight followed by incubation with Alexa Fluor 546-conjugated goat anti-rabbit IgG (1:2000 dilution) for 1 h at RT. The expression levels of Gas6, TNFα, and cleaved caspase 3 were imaged on an Olympus FX1200 confocal laser scanning microscope.

***En face* staining of mouse aortas**

We performed *en face* staining of mouse aortic arches at the greater curvature area, as described in our previous reports[11, 20, 21]. Fluorescent images were obtained using an Olympus FX1200 confocal laser scanning microscope

Serum lipid profile analysis

Mice fasted overnight were euthanized with CO_2; whole blood was collected in a 1.5-ml tube. Whole blood was allowed to clot for 45 min at RT and centrifuged at 1,500xg for 30 min at 4°C. The levels of cholesterol (high- and low-density lipoprotein [HDL and LDL, respectively]) were determined using a cholesterol assay kit for mice (cat #EHDL-100, Bioassay System, USA).

Tissue preparation, histologic evaluation, and quantification of the lesion size in a conventional atherosclerosis model in mice with the background of *Ldlr*$^{-/-}$

WT-*p90rsk*-MTg/*Ldlr*$^{-/-}$ and NLC/*Ldlr*$^{-/-}$ male mice were fed a HFD for 12 or 16 weeks, and killed by CO_2 inhalation. The arterial tree was perfused via the left ventricle with saline containing heparin (40 USPU/mL), followed by 10% neutral buffered formalin in PBS for 10 min. The full length of the aorta from the heart to the iliac bifurcation was dissected and opened along the ventral midline. *En face* preparations were washed in distilled water, dipped in 60% isopropyl alcohol, and stained for 40 min with 0.16% Oil-Red-O dissolved in 60% isopropyl alcohol/0.2 M NaOH. Stained images were captured with a digital camera mounted on a Leica stereomicroscope and analyzed using Adobe Photoshop Extended software.

The aortic sinus area attached to the heart was dissected after fixation, as described earlier, and then embedded in paraffin, and sections (5 μm) were cut. To quantify necrotic core formation, serial sections were made through the entire aortic valve area and stained with hematoxylin and eosin, and the necrotic core area was quantified by the percentage of the non-cellular area/total lesion area using

ImageJ software (http://imagej.nih.gov/ij/). We conducted a double-blind, randomized study, and the persons who evaluated the size of the plaque were blinded to the origin of the sample.

***In situ* TUNEL assay**
The aortic valve area was fixed, embedded in paraffin, and sectioned (5 μm). TUNEL staining was performed using the ApopTag peroxidase *in situ* apoptosis detection kit (#S7100, Millipore), following the manufacturer's protocol, as we previously described[22].

Annexin V apoptosis assay
Cells were stained with annexin V-fluorescein isothiocyanate (annexin V-FITC apoptosis detection kit, cat #ab14085, Abcam, Cambridge, MA), according to the manufacturer's instructions. Annexin V-positive cells were quantified using a BD Accuri C6 Flow Cytometer and the FlowJo software program.

Statistical analysis
The descriptive characteristics are summarized in Supplemental Table 1. Percentages and frequencies were reported for discrete variables; means and standard deviations were reported for continuous characteristics. Fisher's exact test was used to compare the proportions of categorical variables such as sex and race between the HIV^+ and control groups. Welch's *t*-test was used to compare the mean values of continuous variables, such as age and the Reynolds risk score, between the HIV^+ and control groups. For multi-group comparisons, we performed one-way ANOVA, followed by Bonferroni *post hoc* testing, for multiple group comparisons. When groups exhibited unequal variances, Welch's ANOVA was used to perform multiple group comparisons.

Pearson's correlation analysis was used to assess the associations between the Reynolds risk score and plaque formation. Multivariate linear regression was used to model the associations between covariates and continuous outcome variables such as p90RSK activations, controlling for possible confounding effects such as the Reynolds risk score. Regression *t*-tests were used to assess the significance of the linear association between the covariates and the outcome variables. Multivariate logistic regression was used to model the associations between covariates and categorical outcome variables such as the presence of plaques, controlling for possible confounding effects. The Wald test was used to assess the significance of the association between the covariates of interest and the outcome variables. p values <0.05 were considered statistically significant and are indicated by an asterisk in the figures. p values <0.01 are indicated by two asterisks.

For statistical analysis *in vitro* and in animals, differences between two independent groups were determined using the Student *t*-test (two-tailed) and, when applicable, one-way analysis of variance followed by Bonferroni post hoc testing for multiple group comparisons using GraphPad Prism (GraphPad Software, SanDiego). When groups exhibited unequal variances, Welch's analysis of variance was used to perform multiple group comparisons. p values less than 0.05 were considered statistically significant and are indicated by one asterisk in the figures. p values < 0.01 are indicated by two asterisks. All continuous variables were assumed to be normally distributed. Since a large number of statistical comparisons was performed, all at the 0.05 level of significance may result in the possibility of a type I error.

All analyses were performed using R 3.3.0 (R Foundation for Statistical Computing, Vienna, Austria), SAS 9.3 (SAS Institute, Cary, NC, USA), and Prism 5.0 (GraphPad Software, La Jolla, CA, USA) software.

Supplementary data and discussion

Glagov's effect and cART

We investigated the outward remodeling in both groups. As shown in Supplemental Fig. 11, we found no significant difference of outward remodeling between vehicle and cART-treated groups, suggesting that Glagov's effect is maintained in these two groups. It is possible that cART's effects on macrophage function are more critical than is endothelial dysfunction. Therefore, the ability of Glagov's effect has been intact. Further investigation will be necessary to clarify these issues.

Viremia, plaque, and p90RSK activity in our clinical study

It is important to determine how persistent viremia is related to inflammation and atherogenesis. By inclusion criteria, participants were on stable antiretroviral drugs and thus a small percentage of them had low detectable viremia, specifically only 11 patients. Therefore, it is difficult to obtain any conclusive results from our study population but it appears that mild viremia was not associated with both increased activation of p90RSK and plaque formation. In fact, we conducted a Fisher's exact test that included the 11 participants with detectable viremia to determine whether there was a significant association between viremia and carotid plaque (both sides). We did not find any statistical association between these two variables (Supplemental Table 6).

Inflammation in HIV$^+$ patients: other potential mechanisms

We believe that p90RSK is not the only mechanism that leads to inflammation in HIV$^+$ patients. For example, recently the contribution of cGAS-STING-IRF3 pathway in myeloid dendric cells in HIV infection was reported, which can upregulate myeloid cells inflammation[23]. Therefore, the cGAS-STING-IRF3 pathway may play more important role than p90RSK signaling. Of note, the relationship between p90RSK and the cGAS-STING-IRF3 pathway remains unclear. Further investigation will be necessary to clarify these issues.

ROS and p90RSK activation

Although it is well known that p90RSK is a redox-sensitive kinase, the exact molecular mechanism by which p90RSK is activated by ROS remains unclear. It is possible that some phosphatase including PPA2, can be oxidized and lose their activity, which can increase p90RSK activation[24, 25]. However, the inhibition of PP2A activity can also activate many other kinases including p38 and JNK, and it can be difficult to detect the specific role of ROS-mediated p90RSK activation by modifying PP2A activity. It is possible to detect the binding site of p90RSK and PP2A, and generate the mutations or binding inhibitory fragments, which specifically inhibits p90RSK-PP2A binding, and determine the role of oxidized PP2A on p90RSK activation, but this will be beyond the scope of this study.

The roles of antiviral drugs and HIV in plaque formation

The clinical data without the in vitro and animal data could be questioned as it is difficult to completely disentangle the roles of antiviral drugs and HIV. In addition, we could not have a group of cART-treated HIV$^-$ individuals and non-treated HIV$^+$ individuals groups because of ethical issues. However, we performed analyses that separately evaluated those with viremia, a very small sample of 11 participants with detectable viremia in the range of 50-200 copies/ml, vs. no viremia; mild viremia did not increase the level of p90RSK activity, as shown in the Fig. 1g and h. We believe that this in combination of in vitro and animal data strengthens our conclusions that cART-induced p90RSK activation can be an important risk factor for future atherosclerosis-related vascular events.

Supplemental Figure Legends

Supplemental Figure 1. Various cART regimens increase p90RSK activity, which then phosphorylates ERK5 S496, but not the TEY motif, in a time- and dose-dependent manner.
BMDMs from C57Bl/6 mice were treated with various cART regimens for various lengths of time (kinetics, 10 μM each) and also with varying concentrations (dose response) for 10 min in (a, b: ATV [protease inhibitor], c, d: RTV [protease inhibitor], e, f: MVC [CCTR5 antagonist], g, h: RPV [NNRTI], i: TDF/FTC [NRTI; 10 μM each], j: RGV [integrase inhibitor], k, l: EVG [integrase inhibitor]), and Western blotting was performed using specific antibodies against the proteins indicated on the right. The graph represents densitometry data from three independent experiments. Data are mean±SD. **p<0.01.

Supplemental Figure 2. The time-updated CD4 counts and Reynolds risk score show no correlation with p90RSK activity.
(a, b) Pearson correlation tests revealed that there was no significant correlation between the time-updated CD4 counts[26] and basal p90RSK activity (a, p=0.909) or H_2O_2-stimulated p90RSK activation (b, p=0.672). (c, d) Pearson correlation tests showed no significant correlation between the Reynolds risk score and basal p90RSK activity (c, p=0.680) or H_2O_2-stimulated p90RSK activation (d, p=0.223).

Supplemental Figure 3. Various cART regimens inhibit ERK5 transcriptional activity via ERK5 S496 phosphorylation.
(a) BMDMs were transfected with pBind-ERK5 and the Gal4-responsive luciferase reporter pG5-luc, with or without constitutively active MEK5 (CA-MEK5), WT p90RSK (WT-p90RSK), and control pcDNA3.1 vector for 24 h, as indicated. ERK5 transcriptional activity was assayed as described in the Methods. Each data point represents the mean value of a triplicate set of experiments. Mean ± SD., **p<0.01. (b-d) RAW264.7 cells were transfected with pBind-ERK5 and pG5-luc plasmids and pcDNA3.1 plasmid or CA-MEK5 for 30 h; they were then pre-treated with FMK-MEA (10 μM) or vehicle for 1 h, followed by incubation with EFV (10 μM) (b), TDF/FTC/ATV/RTV (10 μM each) (c), TDF/FTC (10 μM each) (c), or vehicle (DMSO, 0.1%) for 6 h. **p<0.01. (d) RAW264.7 cells were transfected with pBind-ERK5 WT, ERK5 S496A mutant (ERK5-S496), pG5-luc, CA-MEK5, or pcDNA3.1 plasmids, as indicated, for 30 h and incubated with TDF/FTC/ATV/RTV (10 μM each) or vehicle (DMSO) for 6 h, and ERK5 transcriptional activity was measured as described in the methods. Mean±SD., **p<0.01, and *p<0.05.

Supplemental Figure 4. Time courses of expression levels of proteins shown in Fig. 2e
The graphs represent densitometry data from three independent gels, one of which is shown in Fig. 2c. (a) Antioxidant molecules expression, (b) NRF2 and CD36 expression, (c) senescence markers expression, and (d) Gas6 and TNFα expression. The data are mean±SD., **p<0.01 and *p<0.05.

Supplemental Figure 5. Expression levels of proteins shown in Fig. 3a.
The graphs represent densitometry data from three independent gels, one of which is shown in Fig. 3a. (a) Antioxidant molecules expression, (b) senescence markers expression, (c) CD36 expression, and (d) Gas6 and TNFα expression. Mean±SD., **p<0.01.

Supplemental Figure 6. cART (TDF/FTC/ATV/RTV) reduces Gas6 expression and increases TNFα and cleaved caspase 3 expression in atherosclerotic plaques.
(a, b) Body weight (a) and HDL and LDL levels (b) in cART- or vehicle-treated *Ldlr*$^{-/-}$ mice. (c-f) The area of atherosclerotic plaques in sections of LCA after PCL was immunofluorescently stained with antibodies against Gas6 (c), TNFα (d), or cleaved caspase 3 (e). Non-immune IgG was used as the control (f). Scale bars: 100 μm except right side of two panels of (c), which were 20 μm. (g) The mean fluorescence intensity of Gas6 and TNFα signals from the whole area (intima and media) was obtained using ImageJ software (left and center), and the percentage ratio of cleaved caspase 3-positive cells relative to total cells (as detected by DAPI) was determined (right). Mean ± SD **p<0.01, *p<0.05. (h) PE macrophages isolated from NLC and WT-*p90rsk*-MTg mice were stained with annexin V-FITC, and labeled cells were quantified on the basis of flow cytometric measurements. Data are presented as mean±SD.

Supplemental Figure 7. Body weights and serum cholesterol levels in WT-*p90rsk*-MTg mice, and peripheral blood cell numbers in DN-*p90rsk*-MTg.
(a, b) Body weight (a) and HDL and LDL levels (b) in WT-p90rsk-MTg/*Ldlr*$^{-/-}$ and control wild type/*Ldlr*$^{-/-}$ mice. (c) Peripheral blood cell counts in NLC and DN-*p90rsk*-MTg mice. The data are mean±SD., **p<0.01 and *p<0.05.

Supplemental Figure 8. Expression levels of proteins shown in Fig. 7g and h.
The graphs represent densitometry data from three independent gels, two of which are shown in Fig. 7g and h. Data on proteins shown in Fig. 7g are presented in graphs above the dotted line while those in Fig. 7h are below the dotted line. (a, e) Antioxidant molecules expression, (b, f) CD36 expression, (c, g) senescence markers expression, (d, h) Gas6 and (d)TNFα expression. Mean±SD., **p<0.01 and *p<0.05.

Supplemental Figure 9. Body weights and serum cholesterol levels, and cART-induced EC inflammation in DN-*p90rsk*-MTg mice.
(a, b) Body weight (a) and HDL and LDL levels (b) in DN-*p90rsk*-MTg and control C57Bl/6 mice after 8 weeks of AAV/D377Y-mPCSK9 injection and a high-fat diet. (c) Wild type (C57BL/6 mice) and DN-*p90rsk*-MTg mice were fed a normal chow and treated twice (20 h and 4 h before euthanasia) with cART (TDF/FTC/ATV/RTV). Aortas were harvested from these mice, and *en face* preparations were double-stained with anti-VE-cadherin (green) and anti-VCAM-1 (red), followed by DAPI staububg. cART increased VCAM-1 expression in NLC, but not in DN-*p90rsk*-MTg mice. Scale bar: 20 μm. Representative images out of five independent experiments are shown. (d) The mean intensity of anti-VCAM-1 staining of the endothelium was determined using ImageJ software. Mean±SD. n = 5, **p<0.01, *p<0.05. Each dot represent the mean intensity from one animal.

Supplemental Figure 10. Outward remodeling of the plaque area is similar between vehicle- and cART-treated mice.
Outward remodeling seen in the gross vessel morphology was evaluated by taking the ratio (%) between outward remodeling area (blue) and total plaque area using ImageJ. The graph shows no difference between the two groups.

Supplemental Figure 11. Repeatability of p90RSK activity measurement by using flow cytometry

Whole blood from one HIV uninfected healthy individual was treated with five different doses ranging from 100-500 μM H_2O_2 for 4 min at room temperature. Alternatively, blood was treated with 200 μM H_2O_2 at different time points from 0 - 16 min. All treatments were performed in triplicate and used to measure p90RSK activation by flow cytometry. The data were analyzed by One-way ANOVA followed by Bonferroni post hoc testing using Graphpad Prism software. Data are mean ± S.D. **** indicate<0.0001.

Supplemental Tables 1-6

Supplemental Table 1. Demographics and clinical variables.

	HIV$^-$ (n=92)		HIV$^+$ (n=104)		p-value
	n	% or Mean (SE)	n	% or Mean (SE)	
Sex					0.0038
Male	51	55.43	79	75.96	
Female	41	44.57	25	24.04	
Race					0.0004
White	80	86.96	64	61.54	
Black	12	13.04	32	30.77	
Other	0	0	4	3.85	
Unknown	0	0	4	3.85	
Current smoker					<0.0001
Yes	6	6.52	34	32.96	
No	84	91.30	67	64.42	
Missing	2	2.17	3	2.88	
Viral load detectable status					-
Detectable	0	0	12	11.54	
<20 or NEG	0	0	84	80.77	
Missing	0	0	8	7.69	
Category					-
NRTI	0	0	1	0.96	
NNRTI	0	0	23	22.12	
Integrase inhibitors	0	0	24	23.08	
Multi-category	0	0	56	53.85	
Family history heart disease					0.0548
Yes	55	59.78	45	43.27	
No	34	36.96	51	49.04	
Unknown	3	3.26	8	7.69	
Bilateral carotid plaques					0.3463
Positive	26	28.26	37	35.58	
Negative	57	61.96	58	55.77	
Missing	9	9.78	9	8.65	
Age	92	59.15 (0.76)	104	55.68 (0.63)	0.0006
Reynolds risk score	83	3.89 (0.34)	94	5.43 (0.38)	0.003
Cholesterol	90	208.99 (21.76)	99	194.51 (4.76)	0.5171
HDL	90	64.73 (2.37)	99	59.9 (3.93)	0.2936
High-sensitivity CRP	90	2.11 (0.64)	98	4.01 (0.8)	0.0646
Sitting systolic	90	122.98 (1.11)	96	126.57 (1.53)	0.0585
CD4 at visit (cells/μL)	-	-	99	745.24 (32.91)	-
Nadir CD4 before entry (cells/μL)	-	-	94	217.85 (16.85)	-
Viral load at visit (copies/mL)	-	-	12	60.42 (11.78)	-
HIV duration (years)	-	-	97	17.73 (0.88)	-
HIV duration (months)	-	-	97	214.94 (10.48)	-

Reported *p* values are based on Fisher's exact test if the variable is categorical or Welch *t*-test if it is continuous.

Abbreviations: CRP, C-reactive protein; NEG, negative (undetectable); NRTI, nucleoside reverse transcriptase inhibitor; NNRTI, non-NRTI; HDL, high-density lipoprotein; HIV, human immunodeficiency virus.

In addition to the NRTI backbone, the multi-category included two or more drugs belonging to more than one category.

Supplemental Table 2. Comparing p90RSK activation among three cART regimens: NNRTI (n=20), integrase inhibitor (n=22), and multi-category (n=49) by one-way ANOVA *F*-test.

	NNRTI	Integrase inhibitor	Multi-category	p-value
Basal p90RSK activation	1.1512±0.347	1.864±0.738	3.895±1.955	0.2794
p90RSK activation after H_2O_2	7.475±1.627	12.633±3.748	9.131±2.051	0.8323

Only one subject used the NRTI regimen; therefore, it was not included in the analysis. No significant differences were detected.

Supplemental Table 3. Univariate logistic regression analysis with the plaque formation.

	Odds ratio	CI 2.5%	CI 97.5%	p-value
Basal p90RSK activation	0.989	0.903	1.045	0.7279
p90RSK activation after H_2O_2	1.007	0.977	1.037	0.6247
Reynolds risk score	1.084	0.987	1.195	0.0944
HIV status	1.458	0.761	2.818	0.2578

Univariate logistic regression analysis show no significant correlation between the formation of plaque on both sides of the carotid artery and p90RSK activation, Reynolds risk score, or HIV status. CI: the confidence interval of the odds ratio.

Supplemental Table 4. Multivariate logistic regression analysis with the plaque formation.

	Estimate	**Std. error**	**p-value**
(Intercept)	-0.753	0.381	0.0481
Reynolds risk score	0.0678	0.050	0.1755
Basal p90RSK activation	-0.3381	0.271	0.2117
HIV status	-0.3070	0.432	0.4778
Interaction	0.6165	0.310	**0.0464**

Multivariate logistic regression analysis involving HIV status, Reynolds score, basal p90RSK activation, and their interaction with HIV status revealed that while neither HIV status nor basal p90RSK activation was significantly associated with plaque formation, their interaction was associated with a significant increase in the risk of forming plaques on both sides of the carotid artery.

Supplemental Table 5. Specific primers for mouse *TNFα*, *iNOS*, *Mcp1*, *Gas6*, *Anxa1*, *Tyro3*, *Mertk*, *Mfge8*, and *Arg1*.

Genes	Sequences	
Tnfα (Sigma)	Forward	5' - CATCTTCTCAAAATTCGAGTGACAA - 3'
	Reverse	5' - TGGGAGTAGACAAGGTACAACCC - 3'
Gas6 (Origene, MP205762)	Forward	5' - GAACTTGCCAGGCTCCTACTCT - 3'
	Reverse	5' - GGAGTTGACACAGGTCTGCTCA - 3'
Mfge8 (Origene, MP 208190)	Forward	5' - GAGCAACAGTGCCAAGGAATGG - 3'
	Reverse	5' - ACTGTGGGCTACCTTGTAGGAC - 3'
Mertk (Origene, MP 202617)	Forward	5' - ATCATCCTCGGCTGCTTCTGTG - 3'
	Reverse	5' - ACGACCAGTTGGGAATCCTCCT - 3'
Thbs1 (Origene, MP216930)	Forward	5' - GGTAGCTGGAAATGTGGTGCGT - 3'
	Reverse	5' - GCACCGATGTTCTCCGTTGTGA - 3'
Mcp-1	Forward	5' - CCACTCACCTGCTGCTACTCA T - 3'
	Reverse	5' - TGGTGATCCTCTTGTAGCTCT CC - 3'
Tyro3	Forward	5' - ATGTCCTCATTCCAGAGCAGCAGT - 3'
	Reverse	5' - CGCTTGAGGCAATGATGTCAGCTT - 3'
Anxa1	Forward	5' - ATGGCAATGGTATCAGAATTCCTCAA - 3'
	Reverse	5' - GATGTCTAGTTTCCACCACACAGAG - 3'
inos	Forward	5' - CTGCAGCACTTGGATCAGGAACCTG - 3'
	Reverse	5' - GGGAGTAGCCTGTGTGCACCTGGAA - 3'
Arg-1 (Sigma)	Forward	5' - AAGACAGCAGAGGAGGTGAAGAG - 3'
	Reverse	5' - TGGGAGGAGAAGGCGTTTGC - 3'

Supplemental Table 6. Viremia and plaque formation

	Plaque on both sides (**no**)	Plaque on both sides (**yes**)
Detectable viral load (**no**)	49	30
Detectable viral load (**yes**)	7	4

Estimated odds ratio: **0.934**; p-value: **1.0**.

We conducted a Fisher's exact test that included the 11 participants with detectable viremia to determine whether there was a significant association between viremia and carotid plaque (both sides). We did not find any statistical association between these two variables.

References

1.Cook NR, Paynter NP, Eaton CB, Manson JE, Martin LW, Robinson JG, Rossouw JE, Wassertheil-Smoller S and Ridker PM. Comparison of the Framingham and Reynolds Risk scores for global cardiovascular risk prediction in the multiethnic Women's Health Initiative. *Circulation*. 2012;125:1748-1756, S1-11.

2.Levine M and Ensom MH. Post hoc power analysis: an idea whose time has passed? *Pharmacotherapy*. 2001;21:405-409.

3.Stein JH, Korcarz CE, Hurst RT, Lonn E, Kendall CB, Mohler ER, Najjar SS, Rembold CM, Post WS and American Society of Echocardiography Carotid Intima-Media Thickness Task F. Use of carotid ultrasound to identify subclinical vascular disease and evaluate cardiovascular disease risk: a consensus statement from the American Society of Echocardiography Carotid Intima-Media Thickness Task Force. Endorsed by the Society for Vascular Medicine. *J Am Soc Echocardiogr*. 2008;21:93-111; quiz 189-190.

4.Villani P, Regazzi MB, Castelli F, Viale P, Torti C, Seminari E and Maserati R. Pharmacokinetics of efavirenz (EFV) alone and in combination therapy with nelfinavir (NFV) in HIV-1 infected patients. *Br J Clin Pharmacol*. 1999;48:712-715.

5.Shiomi M, Matsuki S, Ikeda A, Ishikawa T, Nishino N, Kimura M, Kumagai Y and Irie S. Pharmacokinetic and bioequivalence evaluation of single-tablet and separate-tablet regimens for once-daily cobicistat-boosted elvitegravir in healthy Japanese male subjects: A randomized, two-way crossover study. *Clin Pharmacol Drug Dev*. 2015;4:218-225.

6.Molina JM, Peytavin G, Perusat S, Lascoux-Combes C, Sereni D, Rozenbaum W and Chene G. Pharmacokinetics of emtricitabine, didanosine and efavirenz administered once-daily for the treatment of HIV-infected adults (pharmacokinetic substudy of the ANRS 091 trial). *HIV Med*. 2004;5:99-104.

7.Mora-Peris B, Croucher A, Else LJ, Vera JH, Khoo S, Scullard G, Back D and Winston A. Pharmacokinetic profile and safety of 150 mg of maraviroc dosed with 800/100 mg of darunavir/ritonavir all once daily, with and without nucleoside analogues, in HIV-infected subjects. *J Antimicrob Chemother*. 2013;68:1348-1353.

8.Wang L, Soon GH, Seng KY, Li J, Lee E, Yong EL, Goh BC, Flexner C and Lee L. Pharmacokinetic modeling of plasma and intracellular concentrations of raltegravir in healthy volunteers. *Antimicrob Agents Chemother*. 2011;55:4090-4095.

9.Lamorde M, Walimbwa S, Byakika-Kibwika P, Katwere M, Mukisa L, Sempa JB, Else L, Back DJ, Khoo SH and Merry C. Steady-state pharmacokinetics of rilpivirine under different meal conditions in HIV-1-infected Ugandan adults. *J Antimicrob Chemother*. 2015;70:1482-1486.

10.Wang X, Chai H, Lin PH, Yao Q and Chen C. Roles and mechanisms of human immunodeficiency virus protease inhibitor ritonavir and other anti-human immunodeficiency virus drugs in endothelial dysfunction of porcine pulmonary arteries and human pulmonary artery endothelial cells. *Am J Pathol*. 2009;174:771-781.

11.Le NT, Heo KS, Takei Y, Lee H, Woo CH, Chang E, McClain C, Hurley C, Wang X, Li F, Xu H, Morrell C, Sullivan MA, Cohen MS, Serafimova IM, Taunton J, Fujiwara K and Abe J. A Crucial Role for p90RSK-Mediated Reduction of ERK5 Transcriptional Activity in Endothelial Dysfunction and Atherosclerosis. *Circulation*. 2013;127:486-499.

12.Englen MD, Valdez YE, Lehnert NM and Lehnert BE. Granulocyte/macrophage colony-stimulating factor is expressed and secreted in cultures of murine L929 cells. *J Immunol Methods*. 1995;184:281-283.

13.Kelesidis T and Schmid I. Assessment of Telomere Length, Phenotype, and DNA Content. *Curr Protoc Cytom*. 2017;79:7 26 1-7 26 23.
14.Maekawa N, Abe J, Shishido T, Itoh S, Ding B, Sharma VK, Sheu SS, Blaxall BC and Berk BC. Inhibiting p90 ribosomal S6 kinase prevents (Na+)-H+ exchanger-mediated cardiac ischemia-reperfusion injury. *Circulation*. 2006;113:2516-2523.
15.Bjorklund MM, Hollensen AK, Hagensen MK, Dagnaes-Hansen F, Christoffersen C, Mikkelsen JG and Bentzon JF. Induction of atherosclerosis in mice and hamsters without germline genetic engineering. *Circ Res*. 2014;114:1684-1689.
16.Ko KA, Fujiwara K, Krishnan S and Abe JI. En Face Preparation of Mouse Blood Vessels. *J Vis Exp*. 2017;(123). doi: 10.3791/55460.
17.Heo KS, Le NT, Cushman HJ, Giancursio CJ, Chang E, Woo CH, Sullivan MA, Taunton J, Yeh ET, Fujiwara K and Abe J. Disturbed flow-activated p90RSK kinase accelerates atherosclerosis by inhibiting SENP2 function. *J Clin Invest*. 2015;125:1299-1310.
18.Ko KA, Wang Y, Kotla S, Fujii Y, Vu HT, Venkatesulu BP, Thomas TN, Medina JL, Gi YJ, Hada M, Grande-Allen J, Patel ZS, Milgrom SA, Krishnan S, Fujiwara K and Abe JI. Developing a Reliable Mouse Model for Cancer Therapy-Induced Cardiovascular Toxicity in Cancer Patients and Survivors. *Front Cardiovasc Med*. 2018;5:26.
19.Satoh K, Nigro P, Matoba T, O'Dell MR, Cui Z, Shi X, Mohan A, Yan C, Abe J, Illig KA and Berk BC. Cyclophilin A enhances vascular oxidative stress and the development of angiotensin II-induced aortic aneurysms. *Nat Med*. 2009;15:649-656.
20.Heo KS, Fujiwara K and Abe J. Disturbed-flow-mediated vascular reactive oxygen species induce endothelial dysfunction. *Circulation journal : official journal of the Japanese Circulation Society*. 2011;75:2722-2730.
21.Heo KS, Lee H, Nigro P, Thomas T, Le NT, Chang E, McClain C, Reinhart-King CA, King MR, Berk BC, Fujiwara K, Woo CH and Abe J. PKCzeta mediates disturbed flow-induced endothelial apoptosis via p53 SUMOylation. *J Cell Biol*. 2011;193:867-884.
22.Heo KS, Cushman HJ, Akaike M, Woo CH, Wang X, Qiu X, Fujiwara K and Abe J. ERK5 activation in macrophages promotes efferocytosis and inhibits atherosclerosis. *Circulation*. 2014;130:180-191.
23.Johnson JS, Lucas SY, Amon LM, Skelton S, Nazitto R, Carbonetti S, Sather DN, Littman DR and Aderem A. Reshaping of the Dendritic Cell Chromatin Landscape and Interferon Pathways during HIV Infection. *Cell Host Microbe*. 2018;23:366-381 e9.
24.Kim SH, Seo MS, Jeon WJ, Yu HS, Park HG, Jung GA, Lee HY, Kang UG and Kim YS. Haloperidol regulates the phosphorylation level of the MEK-ERK-p90RSK signal pathway via protein phosphatase 2A in the rat frontal cortex. *Int J Neuropsychopharmacol*. 2008;11:509-517.
25.Ufelmann H and Schrenk D. Nodularin-triggered apoptosis and hyperphosphorylation of signaling proteins in cultured rat hepatocytes. *Toxicol In Vitro*. 2015;29:16-26.
26.Beckman JA, Duncan MS, Alcorn CW, So-Armah K, Butt AA, Goetz MB, Tindle HA, Sico JJ, Tracy RP, Justice AC and Freiberg MS. Association of Human Immunodeficiency Virus Infection and Risk of Peripheral Artery Disease. *Circulation*. 2018;138:255-265.

Appendix

Collaborators

Jacob Fog Bentzon, MD, PhD
Experimental Pathology of Atherosclerosis Laboratory
CNIC (National Cardiovascular Research Center)

Peter Mariuz MD
Department of Medicine
University of Rochester Medical Center School of Medicine and Dentistry

Michael Keefer MD
Department of Medicine
University of Rochester Medical Center School of Medicine and Dentistry

Michael Mancenido D.O.
Thrillium Health, Rochester NY

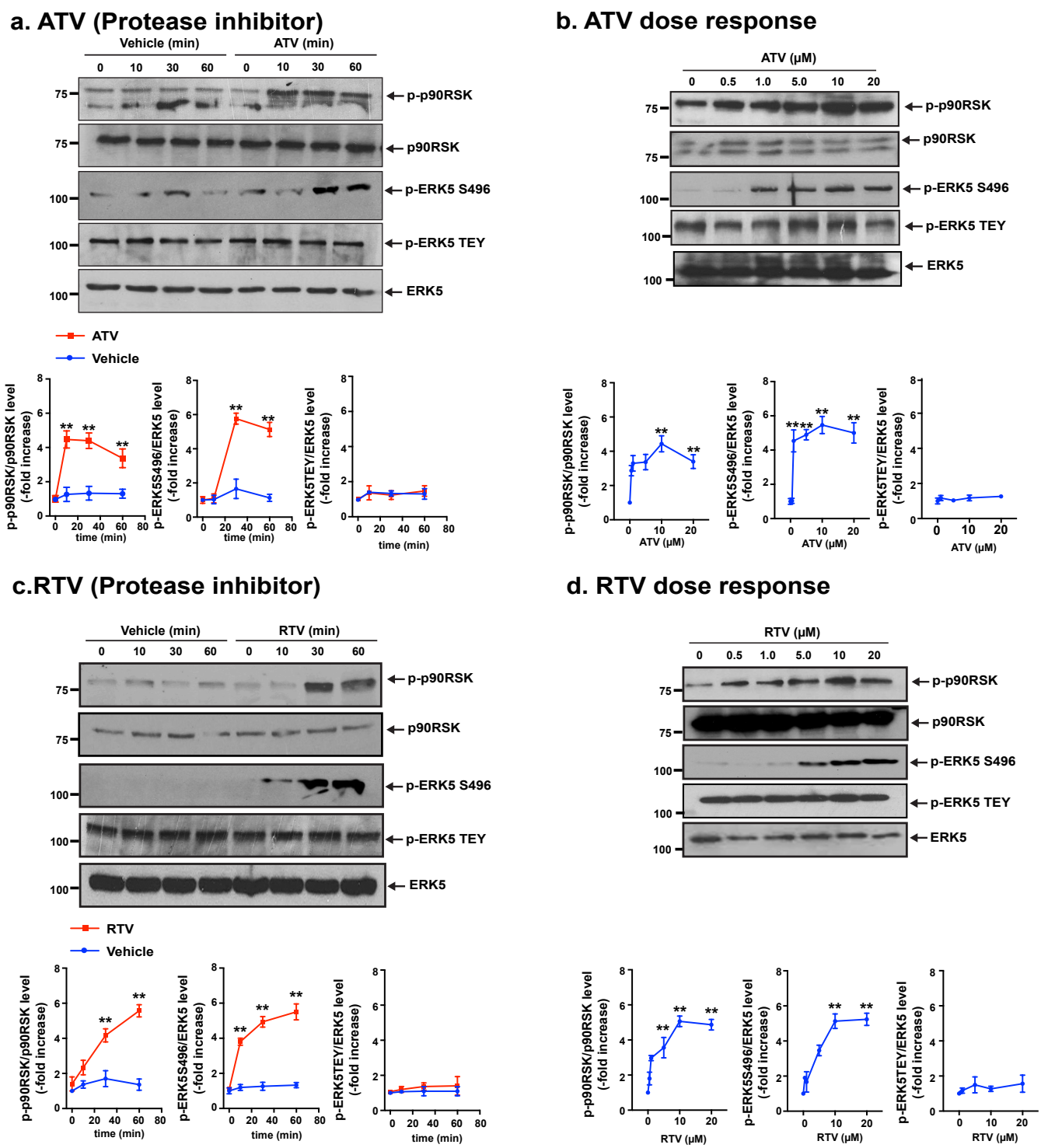
a. ATV (Protease inhibitor)
Vehicle (min)
ATV (min)
0 10 30 60 0 10 30 60
p-p90RSK
p90RSK
p-ERK5 S496
p-ERK5 TEY
ERK5
ATV
Vehicle
p-p90RSK/p90RSK level (-fold increase)
p-ERK5S496/ERK5 level (-fold increase)
p-ERK5TEY/ERK5 level (-fold increase)
time (min)
b. ATV dose response
ATV (μM)
0 0.5 1.0 5.0 10 20
ATV (μM)
c.RTV (Protease inhibitor)
Vehicle (min)
RTV (min)
RTV
Vehicle
d. RTV dose response
RTV (μM)
RTV (μM)

Fig. S1 (1)

e. MVC (CCR5 antagonist)

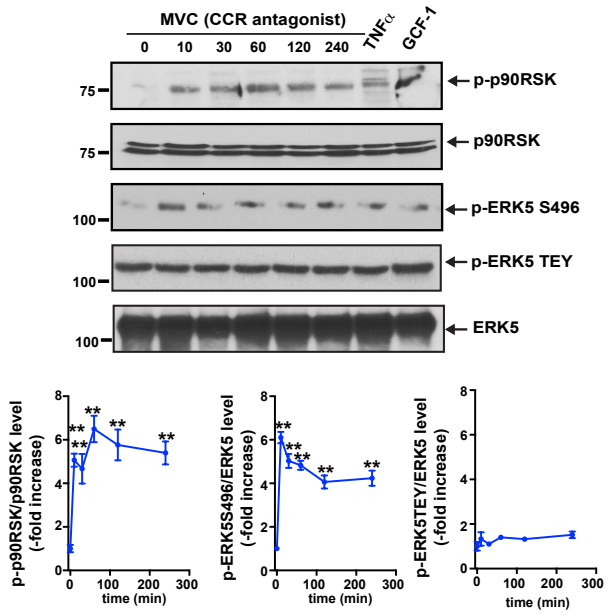

f. MVC dose response

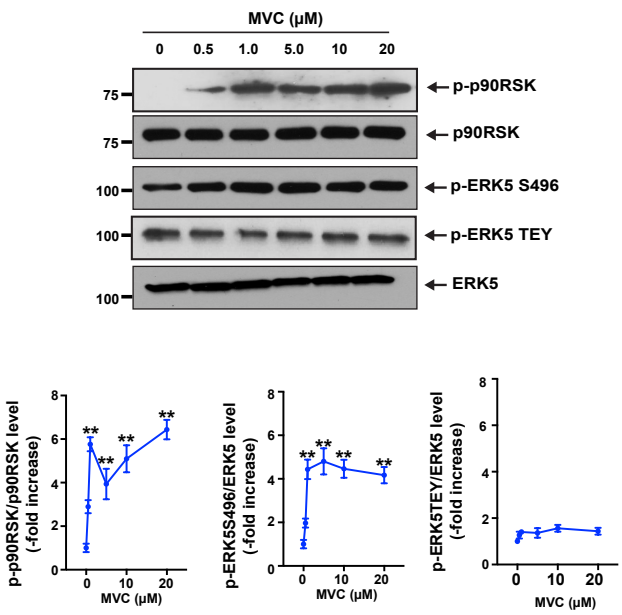

g. RPV (NNRTI)

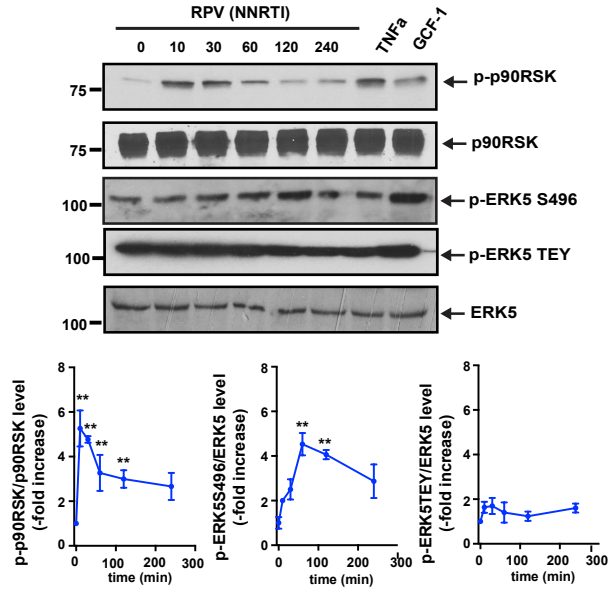

h. RPV dose response

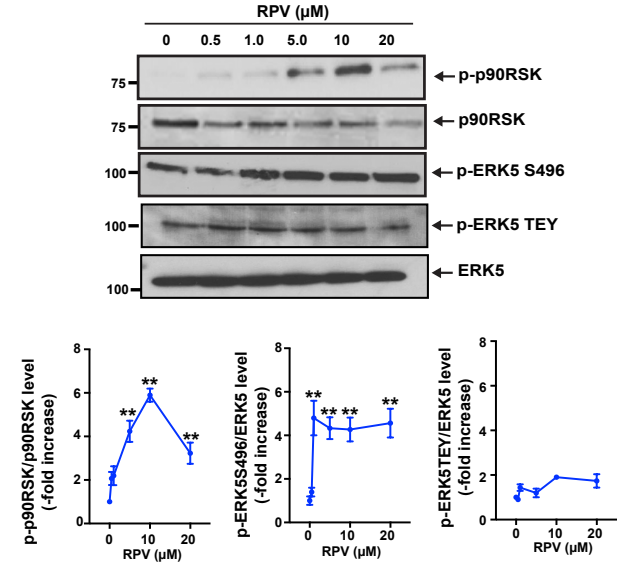

i. TDF/FTC (NRTI)

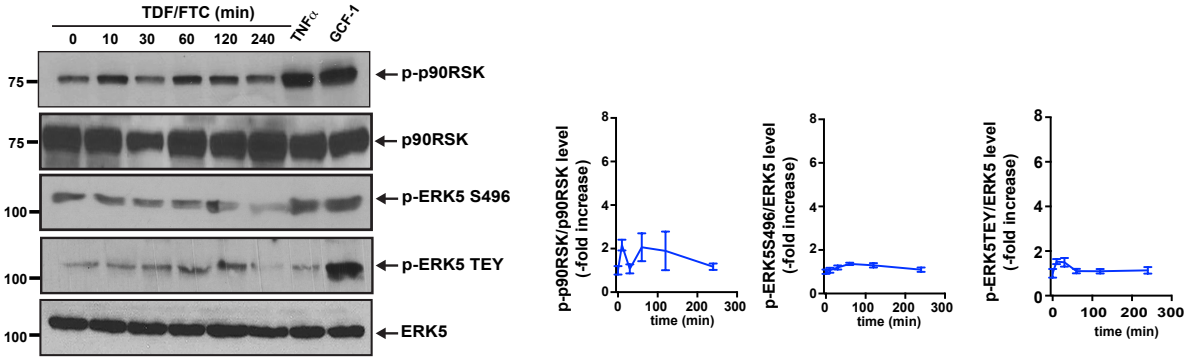

Fig. S1 (2)

j. RGV (Integrase Inhibitor)

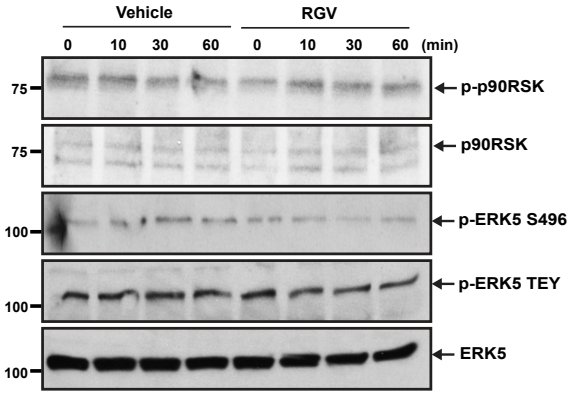

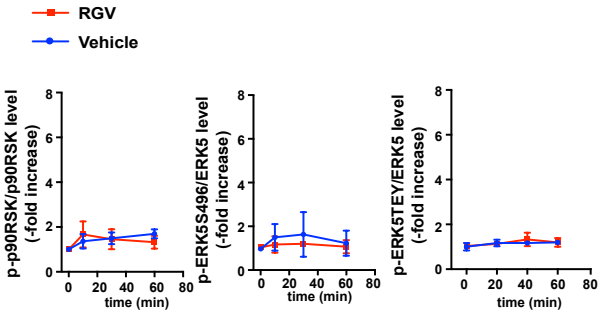

k. EVG (Integrase Inhibitor)

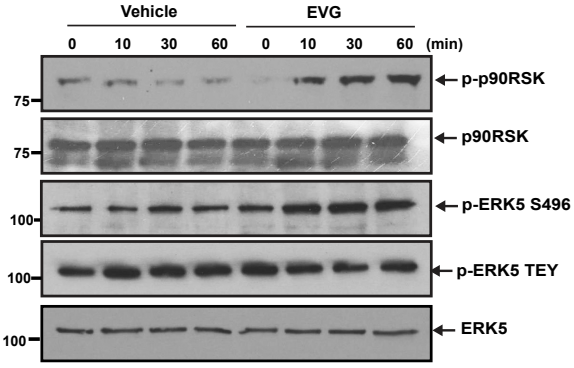

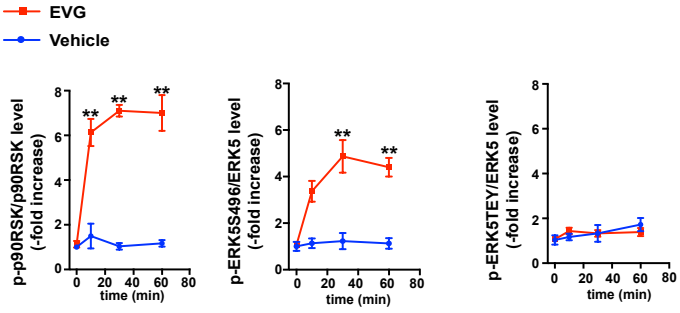

l. EVG dose response

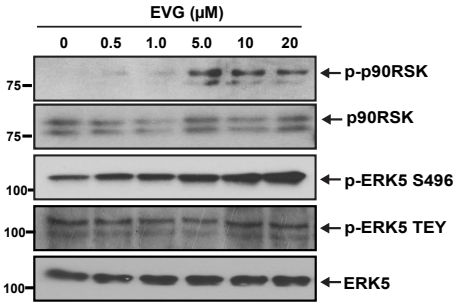

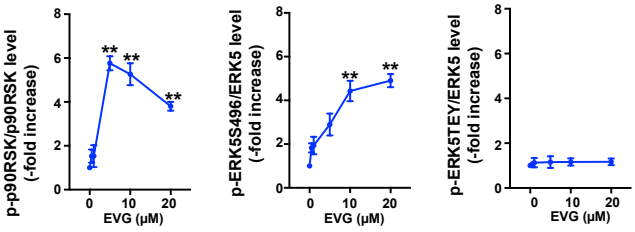

Fig. S1 (3)

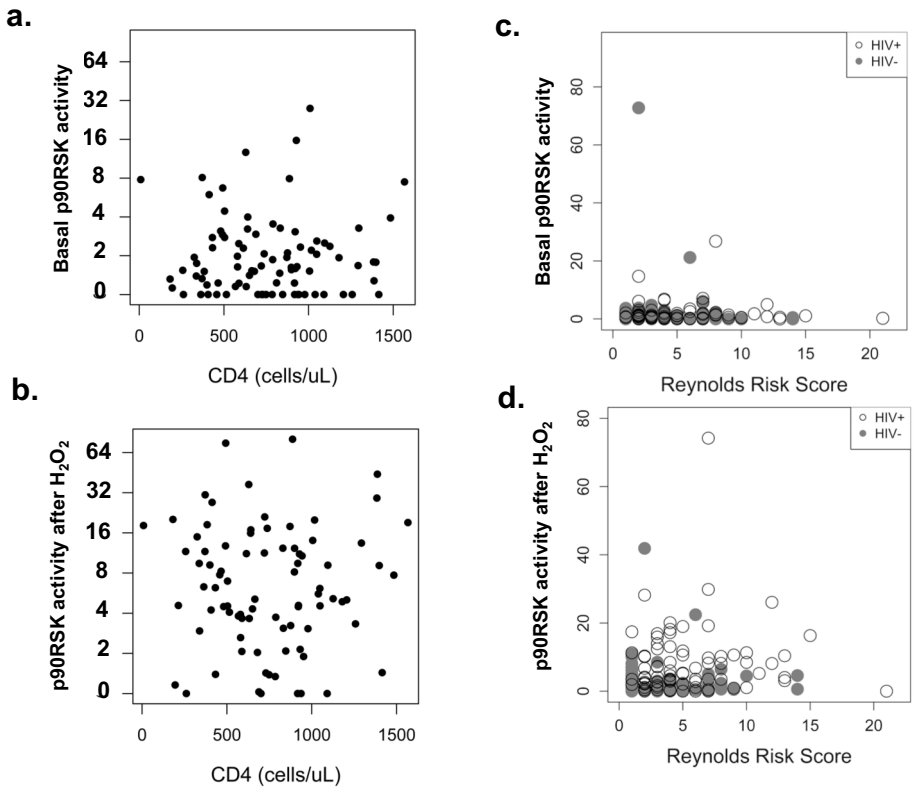
a.
Basal p90RSK activity
64
32
16
8
4
2
0
0
500
1000
1500
CD4 (cells/uL)
b.
p90RSK activity after H_2O_2
64
32
16
8
4
2
0
0
500
1000
1500
CD4 (cells/uL)
c.
Basal p90RSK activity
HIV+
HIV-
0
20
40
60
80
0
5
10
15
20
Reynolds Risk Score
d.
p90RSK activity after H_2O_2
HIV+
HIV-
0
20
40
60
80
0
5
10
15
20
Reynolds Risk Score

Fig. S2

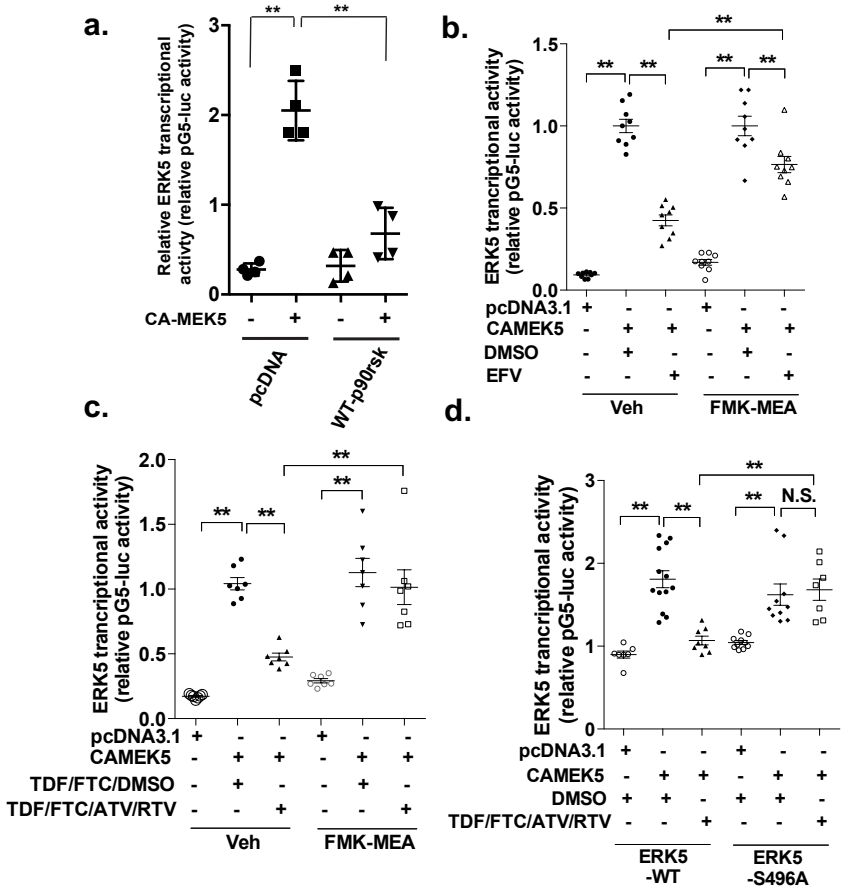
a.
Relative ERK5 transcriptional activty (relative pG5-luc activity)
CA-MEK5
pcDNA
WT-p90rsk
b.
ERK5 trancriptional activity (relative pG5-luc activity)
pcDNA3.1
CAMEK5
DMSO
EFV
Veh
FMK-MEA
c.
ERK5 trancriptional activity (relative pG5-luc activity)
pcDNA3.1
CAMEK5
TDF/FTC/DMSO
TDF/FTC/ATV/RTV
Veh
FMK-MEA
d.
ERK5 trancriptional activity (relative pG5-luc activity)
N.S.
pcDNA3.1
CAMEK5
DMSO
TDF/FTC/ATV/RTV
ERK5 -WT
ERK5 -S496A

Fig. S3

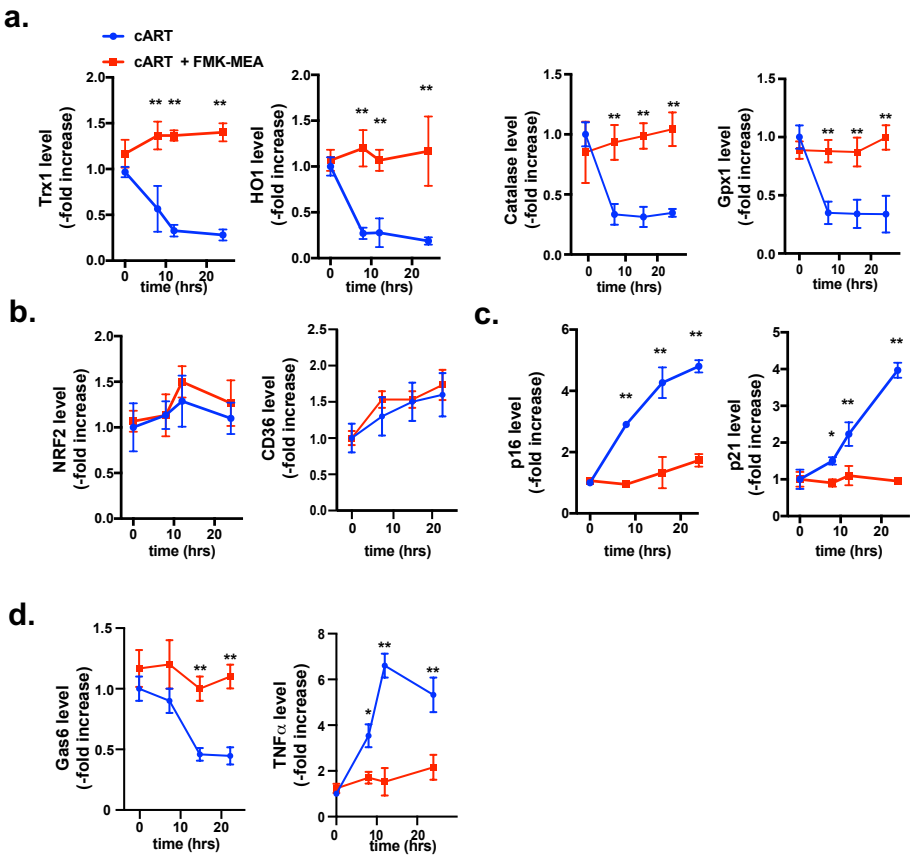
a.
cART
cART + FMK-MEA
Trx1 level (-fold increase)
HO1 level (-fold increase)
Catalase level (-fold increase)
Gpx1 level (-fold increase)
time (hrs)
b.
NRF2 level (-fold increase)
CD36 level (-fold increase)
c.
p16 level (-fold increase)
p21 level (-fold increase)
d.
Gas6 level (-fold increase)
TNFα level (-fold increase)

Fig. S4

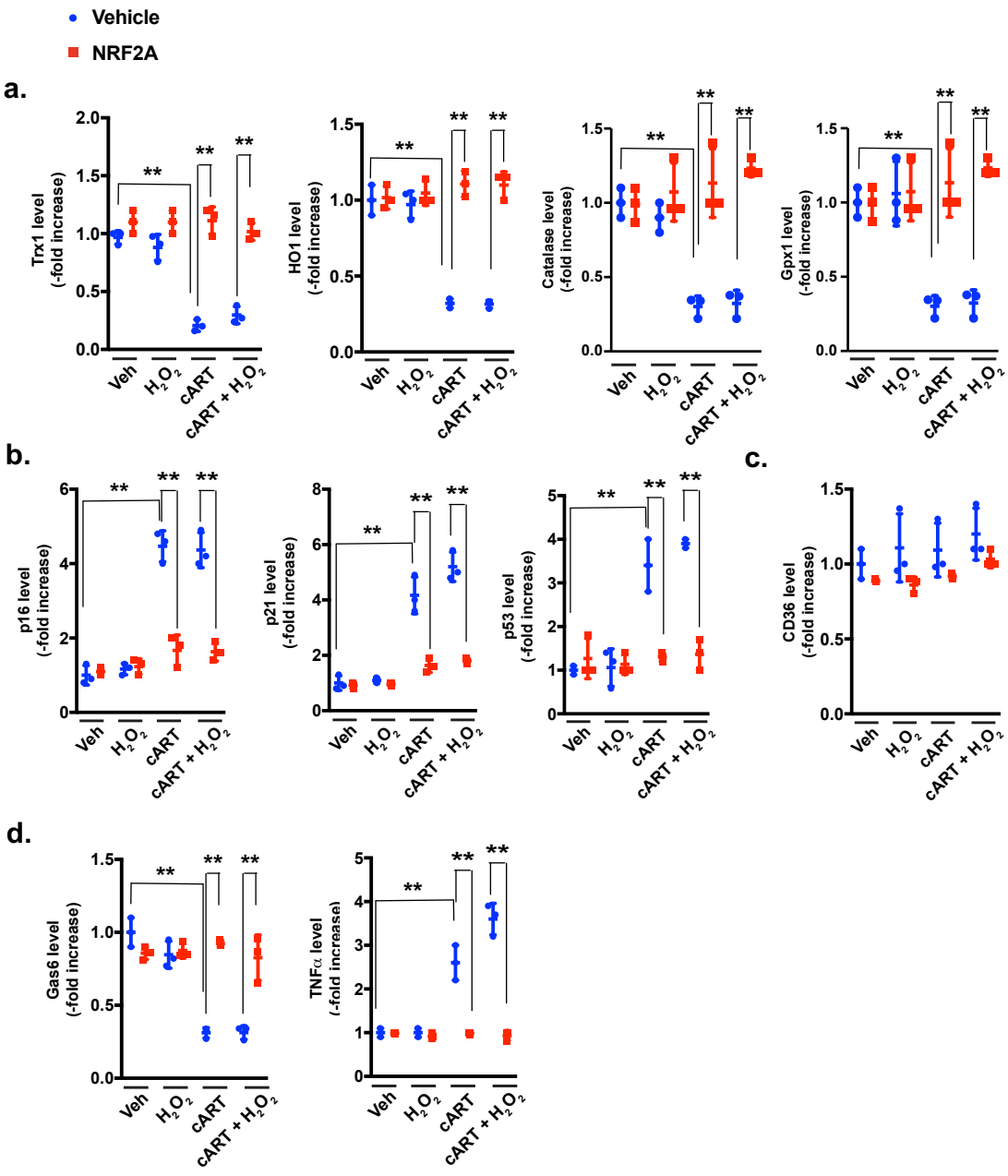
Vehicle
NRF2A
a.
Trx1 level (-fold increase)
HO1 level (-fold increase)
Catalase level (-fold increase)
Gpx1 level (-fold increase)
b.
p16 level (-fold increase)
p21 level (-fold increase)
p53 level (-fold increase)
c.
CD36 level (-fold increase)
d.
Gas6 level (-fold increase)
TNFα level (-fold increase)
Veh
H2O2
cART
cART + H2O2
**

Fig. S5

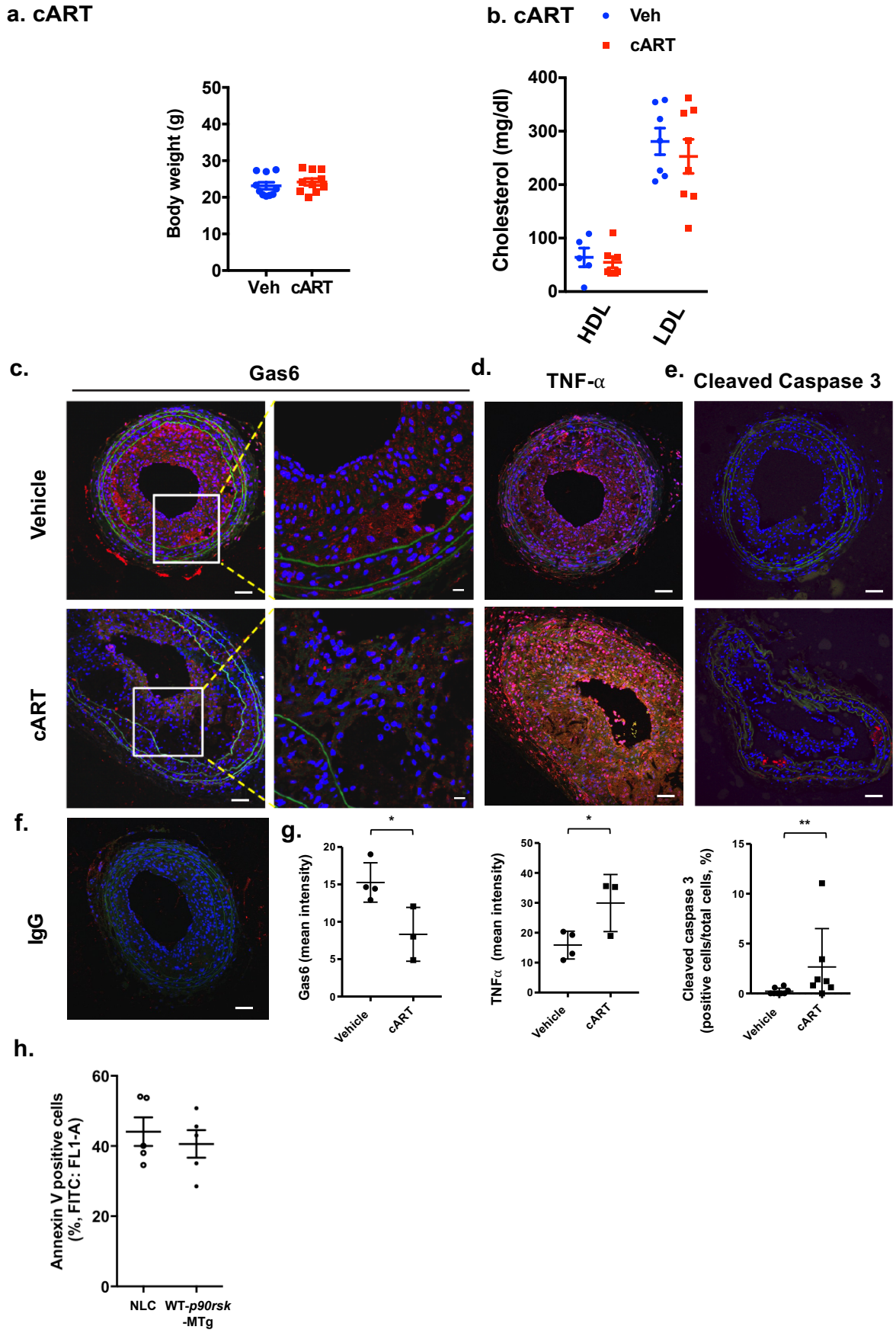
a. cART
Body weight (g)
50
40
30
20
10
0
Veh
cART
b. cART
Veh
cART
Cholesterol (mg/dl)
400
300
200
100
0
HDL
LDL
c.
Gas6
d.
TNF-α
e.
Cleaved Caspase 3
Vehicle
cART
f.
IgG
g.
Gas6 (mean intensity)
20
15
10
5
0
*
Vehicle
cART
TNFα (mean intensity)
50
40
30
20
10
0
*
Vehicle
cART
Cleaved caspase 3 (positive cells/total cells, %)
15
10
5
0
**
Vehicle
cART
h.
Annexin V positive cells (%, FITC: FL1-A)
60
40
20
0
NLC
WT-p90rsk -MTg

Fig. S6

a. WT-*p90rsk*-MTg

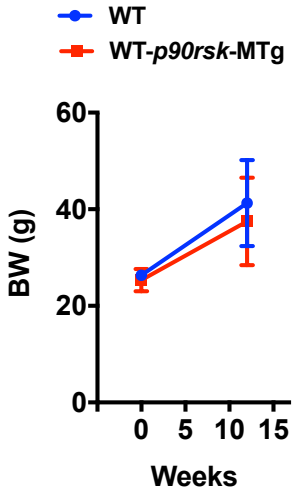

b. WT-*p90rsk*-MTg

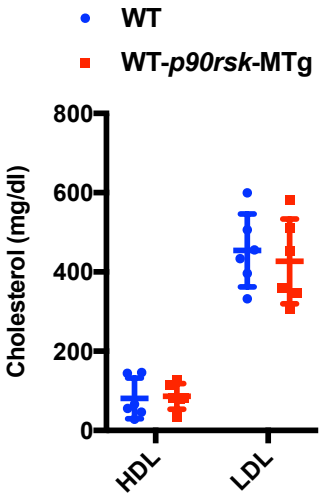

c. DN-*p90rsk*-MTg

Cell types	NLC	DN-p90rsk-MTg
WBCs (x 10^3/µl)	8.57 ± 1.99	7.99 ± 3.24
Lymphocytes (x 10^3/µl)	7.22 ± 1.90	6.81 ± 2.93
Monocytes (x 10^3/µl)	0.13 ± 0.04	0.10 ± 0.05
RBCs (x 10^3/µl)	10.88 ± 0.40	10.97 ± 0.38
Platelets (x 10^6/µl)	0.71 ± 0.10	0.61 ± 0.16

Fig. S7

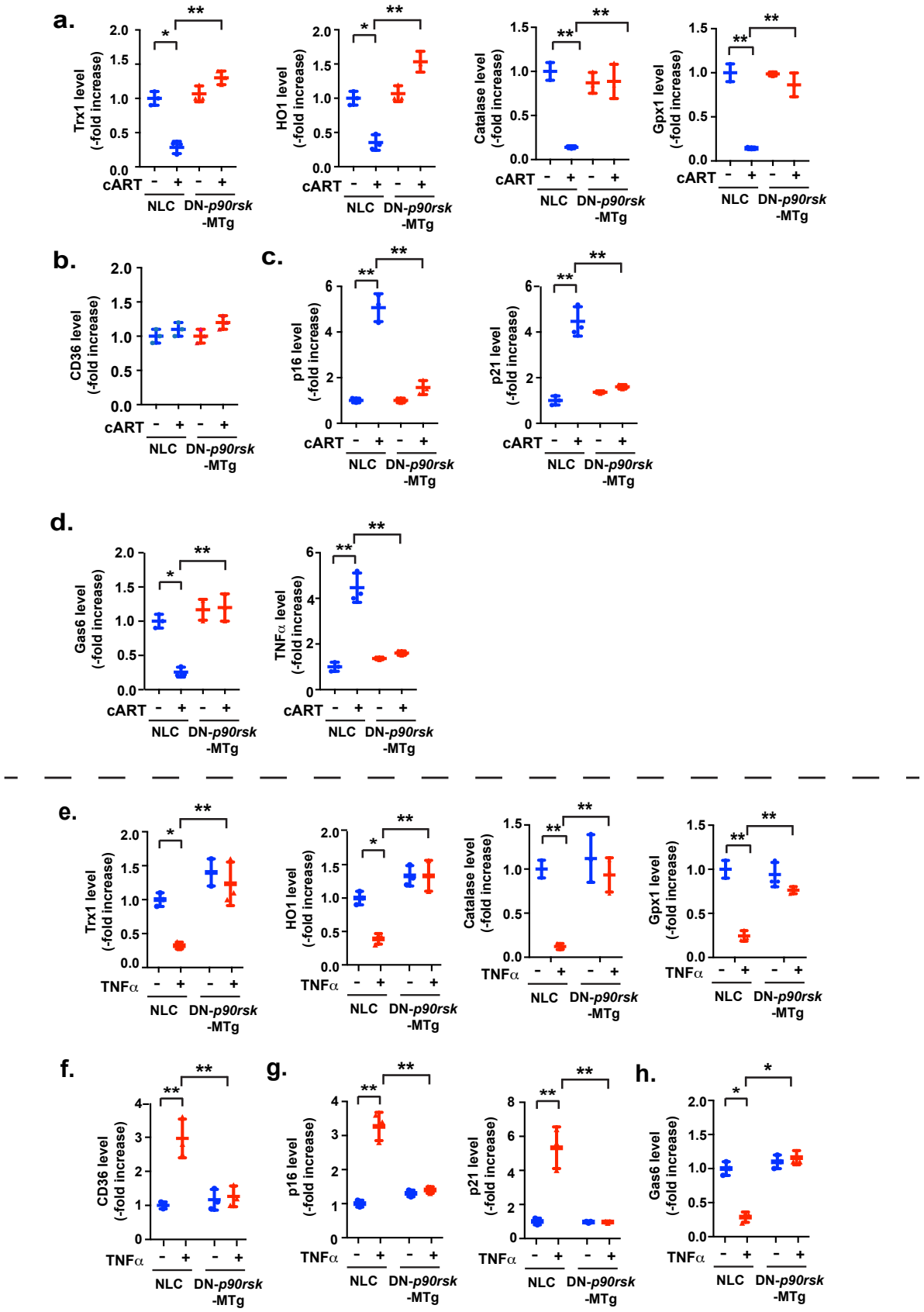
a.
Trx1 level (-fold increase)
HO1 level (-fold increase)
Catalase level (-fold increase)
Gpx1 level (-fold increase)
b.
CD36 level (-fold increase)
c.
p16 level (-fold increase)
p21 level (-fold increase)
d.
Gas6 level (-fold increase)
TNFα level (-fold increase)
e.
Trx1 level (-fold increase)
HO1 level (-fold increase)
Catalase level (-fold increase)
Gpx1 level (-fold increase)
f.
CD36 level (-fold increase)
g.
p16 level (-fold increase)
p21 level (-fold increase)
h.
Gas6 level (-fold increase)
cART
TNFα
NLC
DN-p90rsk -MTg

Fig. S8

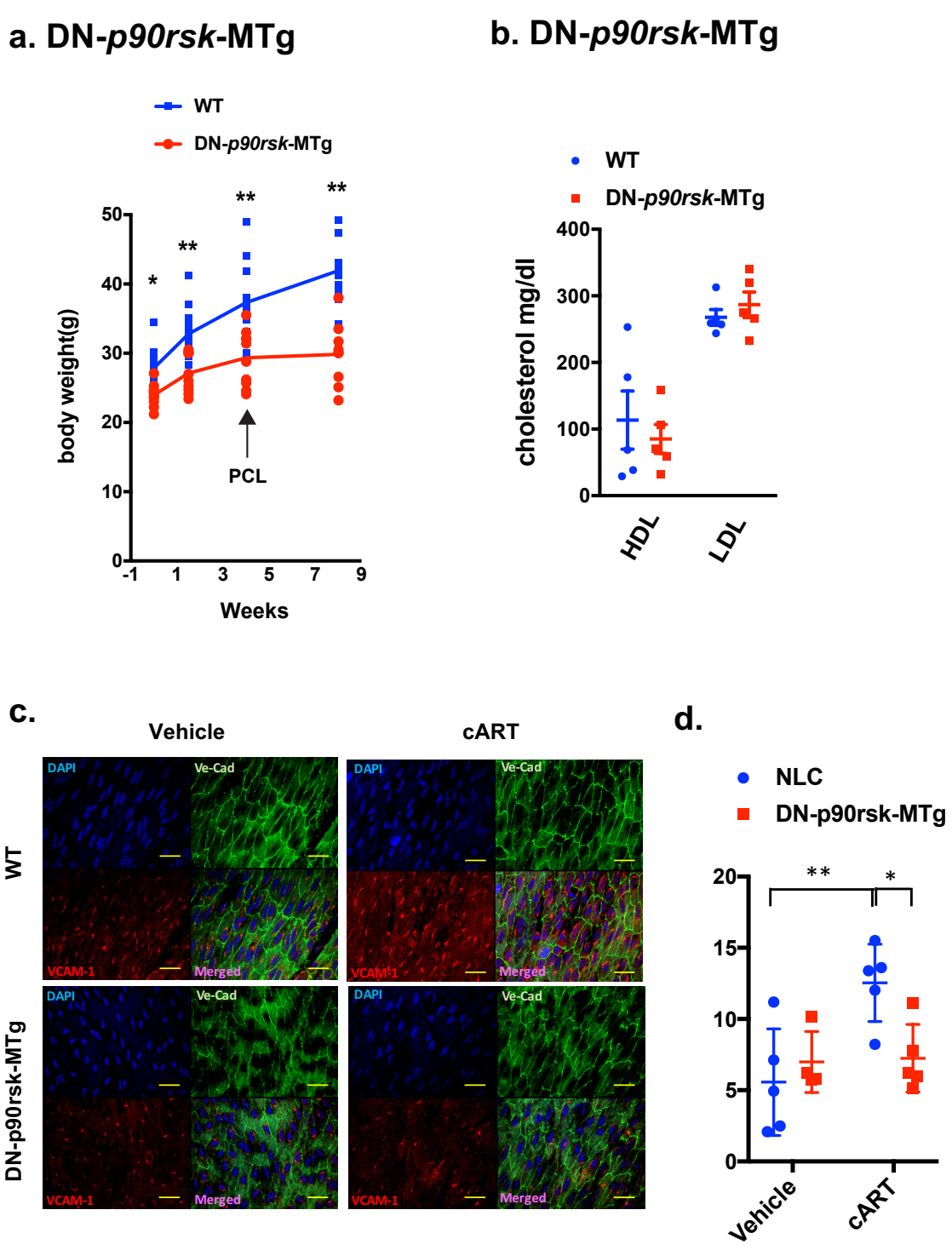
a. DN-p90rsk-MTg
WT
DN-p90rsk-MTg
body weight(g)
Weeks
PCL
b. DN-p90rsk-MTg
WT
DN-p90rsk-MTg
cholesterol mg/dl
HDL
LDL
c.
Vehicle
cART
WT
DN-p90rsk-MTg
DAPI
Ve-Cad
VCAM-1
Merged
d.
NLC
DN-p90rsk-MTg
Vehicle
cART

Fig. S9

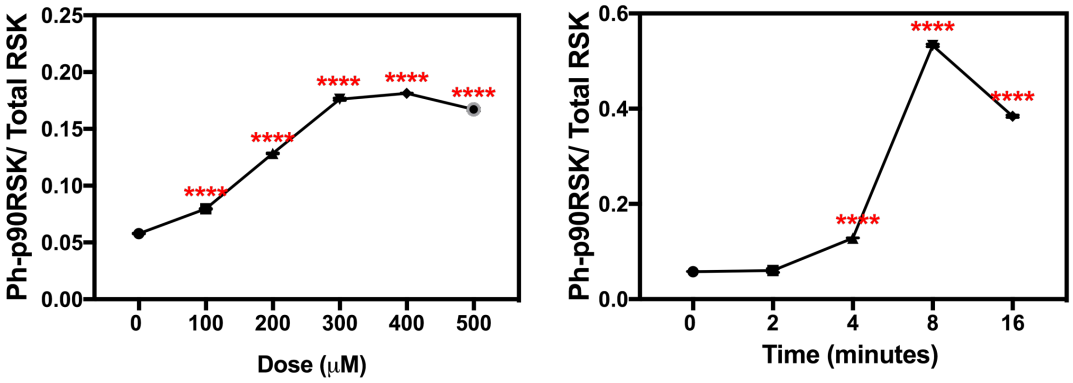
Ph-p90RSK/ Total RSK
0.25
0.20
0.15
0.10
0.05
0.00
0
100
200
300
400
500
Dose (μM)
****
****
****
****
****
Ph-p90RSK/ Total RSK
0.6
0.4
0.2
0.0
0
2
4
8
16
Time (minutes)
****
****
****

Fig. S10

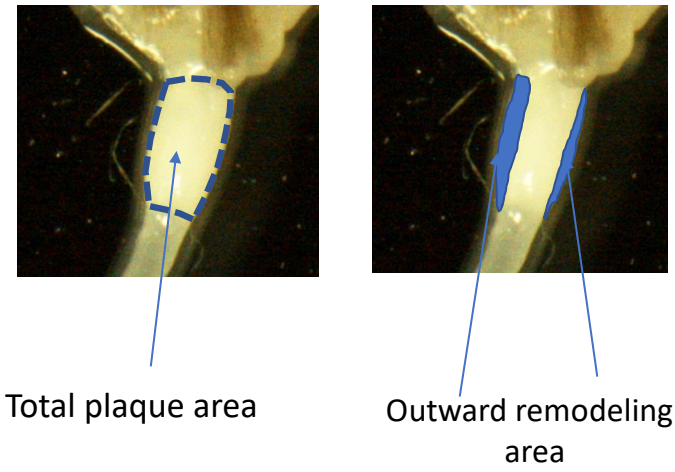
Total plaque area
Outward remodeling area

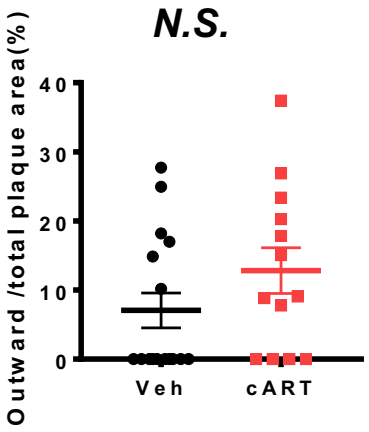
N.S.
Outward /total plaque area(%)
40
30
20
10
0
Veh
cART

Fig. S11